ACS Symp. Ser. 502, 16 (1992).

Chapter 2

Variational Transition-State Theory with Multidimensional, Semiclassical, Ground-State Transmission Coefficients

Applications to Secondary Deuterium Kinetic Isotope Effects in Reactions Involving Methane and Chloromethane

Donald G. Truhlar[1-3], Da-hong Lu[1,3,4], Susan C. Tucker[1,3,5], Xin Gui Zhao[2,3,6], Angels Gonzalez-Lafont[1,3,7], Thanh N. Truong[1,3,8], David Maurice[1,3,9], Yi-Ping Liu[1,3], and Gillian C. Lynch[1,3]

[1]Department of Chemistry, [2]Chemical Physics Program, and [3]Supercomputer Institute, University of Minnesota, Minneapolis, MN 55455–0431

This article has two parts. The first provides an overview of variational transition state theory with multidimensional semiclassical ground-state transmission coefficients. The second provides an update of recent applications to three secondary deuterium kinetic isotope effects in gas-phase C_1 reactions, in particular:

$$H + CD_3H \rightarrow H_2 + CD_3$$
$$^*Cl^- + CD_3Cl \rightarrow CD_3{}^*Cl + Cl^-$$

and

$$^*Cl(D_2O)^- + CH_3Cl \rightarrow CH_3{}^*Cl + Cl(D_2O)^-$$

where *Cl denotes a labeled chlorine atom.

Molecular modeling techniques have allowed for significant progress in the quantitative treatment of kinetic isotope effects (KIEs) for atom-diatom reactions. Both accurate quantum mechanical calculations and generalized transition state theory approaches have been used, and the former have been used to test the latter (*1-9*).

[4]Current address: Department of Chemistry, Fitchburg State College, 160 Pearl Street, Fitchburg, MA 01420
[5]Current address: Department of Chemistry, University of California, Davis, CA 95616
[6]Current address: Fuel Science Program, Department of Materials Science and Engineering, 210 Academic Projects Building, Pennsylvania State University, University Park, PA 16802
[7]Current address: Unidad Quimica Fisica, Departamento Quimica, Universidad Autonoma de Barcelona, Bellaterra 08193 (Barcelona), Spain
[8]Current address: Department of Chemistry, University of Houston, Houston, TX 77204–5641
[9]Current address: Department of Chemistry, University of California, Berkeley, CA 94720

0097–6156/92/0502–0016$06.25/0

Some critical tests against experiment are also available (for one especially relevant example see *10*). The extension of accurate molecular modeling techniques for the chemical dynamics of gas-phase reactions from atom-diatom collisions to polyatomic collisions is a challenge addressed in the present chapter. Our own work in this area has been focused on the generalized transition state theory approach in which quantized variational transition state theory, in particular in either the canonical variational theory (CVT) or improved canonical variational theory form (*11-16*), is combined with a transmission coefficient based on multidimensional semiclassical tunneling calculations and the ground-state transmission coefficient approximation (*13-20*). The present article reviews some of our work for the following set of C_1 reactions:

Reaction		References
(R1)	$H + CH_4 \rightarrow H_2 + CH_3$	(*21-29*)
(R2)	$^*Cl^- + CH_3Cl \rightarrow CH_3{}^*Cl + Cl^-$	(*30-34*)
(R3)	$^*Cl(H_2O)^- + CH_3Cl \rightarrow CH_3{}^*Cl + Cl(H_2O)^-$	(*31-34*)

Note that *Cl denotes a labeled chlorine atom. We will discuss secondary deuterium KIEs for CH_3/CD_3 isotopic substitution in reaction R1 (*27*) and R2 (*30,32-34*) and secondary deuterium KIEs for H_2O/D_2O substitution in R3 (*32-34*). Although the original papers consider a wide range of temperatures in all cases, we restrict our discussion here to 300-700 K for R1 and to 300 K for R2 and R3. We have also calculated secondary deuterium KIEs for CH_3/CD_3 substitution in the reverse of R1 (*27*), in $D + CD_3H \rightarrow HD + CD_3$ (*27*), and in R3 (*32-34*) and for both CD_3 and D_2O substitution in the reaction of $^*Cl(H_2O)_2^-$ with CH_3Cl (*31-33*), but that work is not reviewed here. Similar techniques have also been applied to calculate rate constants for three other reactions of methane, $Cl + CH_4 \rightarrow HCl + CH_3$ (*29*), $OH + CH_4 \rightarrow H_2O + CH_3$ (*35*), and $CF_3 + CH_4 \rightarrow CF_3H + CH_3$ (*36*), but secondary KIEs have not been calculated yet for these reactions. We have also calculated primary kinetic isotope effects for reactions R1 (*23*) and $CF_3 + CH_4 \rightarrow CF_3H + CH_3$ (*36*), but these will not be discussed here.

An important lesson of the work reviewed here is that interpretations of kinetic isotope effects based on conventional theory are often not borne out by the more complete treatments, which are the focus of this review. We will start out by reviewing the conventional theory, and then we will contrast it to the improved theory.

Conventional theory

Kinetic isotope effects are usually interpreted in terms of conventional transition state theory (TST, *37-39*), and tunneling is typically invoked only to explain "anomalous" (large) KIEs. The TST rate expression is

$$k = \kappa\sigma\frac{\bar{k}T}{h}\frac{Q^{\neq}}{\Phi^R}e^{-V^{\neq}/RT} \qquad (1)$$

where κ is the tunneling transmission coefficient (often set equal to unity), σ is a symmetry factor (number of equivalent reaction paths), $\bar{k}$ is Boltzmann's factor, T is temperature, h is Planck's constant, $Q^{\neq}$ is the transition state partition function with the zero of energy at $V^{\neq}$ and one degree of freedom (the reaction coordinate) fixed, Φ^R is the reactant partition function with zero of energy at classical equilibrium for reactants, $V^{\neq}$ is the saddle point potential energy with the zero of energy at classical equilibrium for reactants, and R is the gas constant. All symmetry factors are omitted from

rotational partition functions $Q^{\neq}$ and Φ^R but are included in σ. The per-site KIE is defined as

$$\eta = \frac{k_H/k_D}{\sigma_H/\sigma_D} \tag{2}$$

where k_H denotes the rate coefficient for the unsubstituted reactants, and k_D denotes the rate coefficient when one or more H is changed to D. It is informative to factor η values calculated from (1) as

$$\eta = \eta^{\neq}_{tun}\eta^{\neq} \tag{3}$$

where the tunneling contribution is

$$\eta^{\neq}_{tun} = \kappa_H/\kappa_D \tag{4}$$

and the conventional TST KIE is

$$\eta^{\neq} = \frac{Q^{\neq}_H/\Phi^R_H}{Q^{\neq}_D/\Phi^R_D}. \tag{5}$$

If tunneling is included in conventional TST treatments it is almost always treated as one-dimensional. Then $\eta^{\neq}_{tun} \cong 1$ for secondary KIEs in most organic reactions since this kind of substitution usually has only a small effect on the reduced mass for motion along the reaction coordinate; however in some cases participation of secondary (i.e., non-transferred) hydrogens in the imaginary-frequency normal mode at the saddle point has been invoked in order to use conventional TST to explain anomalously high secondary KIEs that have been observed experimentally (*40-42*). (In conventional one-dimensional models, participation of such secondary hydrogens in the reaction coordinate is *necessary* in order to give a significant isotopic dependence to κ.)

In practice one assumes that rotations and vibrations are separable. Then $\eta^{\neq}$ may be further factored into translational, rotational, and vibrational contributions:

$$\eta^{\neq} = \eta_{trans}\eta^{\neq}_{rot}\eta^{\neq}_{vib}. \tag{6}$$

The traditional way to interpret α-deuterium KIEs in S_N2 reactions focuses on the vibrational contribution $\eta^{\neq}_{vib}$, and in particular on the bending vibrations at the reactive carbon. For a reaction in which the hybridization at the reactive carbon changes from sp^3 to sp^2, the bending force constants are assumed to be reduced, in which case the zero point energy requirement decreases as the system transforms from reactant to transition state. This zero point effect is greater for H than for D, and it is assumed to dominate the KIE; thus k_H is expected to be greater than k_D (*38,39,43*). Conversely, the extent to which k_H exceeds k_D is often used (see, e.g., *44,45*) as a tool for mechanistic analysis; a larger k_H/k_D may be associated with greater sp^2 character at the transition state (an S_N1-like reaction.) The conventional interpretation has been summarized by Saunders (*39*): "A larger k_H/k_D indicates a transition state in which the out-of-plane bend of the α-hydrogen is less encumbered than in the reactants." Wolfsburg and Stern extended this argument to reactions of the type $CH_3X + X \rightarrow CH_3XX^{\neq}$, again emphasizing the HCX bending force constant (*46*). We will see that our calculations indicate that many modes contribute to k_H/k_D so the interpretation is not so clear.

Generalized transition state theory

In the version of generalized transition state theory that we have developed and that we use to analyze KIEs, we still retain the concept of a transition state, but we do not necessarily identify it with the saddle point (highest-energy point on the minimum-energy path from reactants to products). The fundamental property upon which the generalization is based results from the equivalence of the transition state rate expression in classical mechanics to the one-way flux of an equilibrium ensemble of reactants through a hypersurface in configuration space (i.e., a system with one degree of freedom fixed). If we retain the assumption of reactant equilibrium, which is apparently often reasonable, even for fast reactions, under typical experimental conditions, as discussed elsewhere (*47*), then the one-way flux is an upper bound to the net rate and becomes exact when the transition state is a perfect dynamical bottleneck, i.e., when all trajectories cross the transition state at most once, which is called the no-recrossing assumption (for a pedagogical discussion see *16*). Although the variational bound and convergence to the exact result as the variational optimization is improved are both lost in a quantum mechanical world (*48*), our working procedure is to vary the location of the transition state hypersurface to minimize the rate at a given temperature (i.e., for a canonical ensemble), even though we use quantized vibrational partition functions. Since the reaction coordinate is missing (i.e., fixed) in the generalized transition state vibrational partition function, quantum effects on the reaction coordinate are included in a transmission coefficient which is based on a semiclassical multidimensional tunneling (MT) correction to the CVT prediction for the ground state of the transition state and hence is called κ^{MT}. This leads to canonical variational theory with a semiclassical-tunneling ground-state transmission coefficient; the resulting rate constant expression is written

$$k^{CVT/MT} = \kappa^{MT}\sigma\frac{kT}{h}\frac{Q^{CVT}}{\Phi^R}e^{-V^{CVT}/RT} \tag{7}$$

where Q^{CVT} is the generalized transition state partition function at the optimized location with zero of energy at the classical equilibrium geometry of this generalized transition state, and V^{CVT} is the potential energy at this point. Again all symmetry factors are in σ.

Details of the practical implementation of these equations are given elsewhere (especially *13*). A critical aspect is the way in which the variational transition state definition and optimization is made practical. To search for the best variational transition state as an arbitrary (3N-4)-dimensional hypersurface (for an N-atom system) corresponding to fixed center of mass and fixed reaction coordinate would require, first, that one is able to calculate quantized partition functions (Q^{CVT}) for arbitrarily shaped hypersurfaces and, second, that one is able to perform a multidimensional optimization of a large number of variables required to define such a surface. Instead we define a one-parameter sequence of physically motivated generalized transition states orthogonal to a reaction path (the distance along the reaction path is the reaction coordinate s, and the parameter is the value of s at which the generalized transition state, i.e., the hypersurface, intersects s) for which the partition function may be calculated by standard methods, and we optimize the transition state within this sequence. In particular the reaction path is taken to be the minimum-energy path (MEP) in mass-scaled cartesian coordinates (*49-53*), and the shape of the hypersurface off the MEP is defined simply in terms of internal coordinates or cartesian vibrations. Although it is not clear *a priori* that the best transition state in this set is good enough, we have obtained very accurate results for cases where the theory can be tested against accurate

quantum mechanics (*1-8*) and reasonable results in other cases, and so we accept this as good enough. [Further discussion of the shape of the generalized transition state hypersurfaces off the MEP is provided elsewhere (*28*), where in particular we emphasize that this choice is equivalent to choosing a definition of s for points off the MEP.] In the present calculations we also make the harmonic approximation for all vibrational partition functions.

Since, as discussed above, our extension of variational transition state theory to the quantum mechanical world is not rigorous, the usefulness of the approximation scheme must be tested by comparison to accurate quantum dynamics, which is only feasible at present for atom-diatom reactions, or to experiment. Since comparison to experiment is clouded by uncertainties in the potential energy function, we have relied on comparison to accurate quantum dynamics. Extensive comparisons of this type have been carried out (*1-8,12-20*), and they generally confirm the accuracy of our quantized approach. Thus we hope that applications to polyatomics, such as provided here, may be viewed as testing the potential rather than the dynamical theory. One should not forget though that the theory may be less accurate for new reactions than for the reactions for which it has been tested.

The most important question to be addressed in this regard is recrossing. Variational transition state theory does not include recrossing for the best variational transition state. In principle the transmission coefficient should account for such effects, i.e., for classical trajectories that cross the variational transition state in the direction of products but do not proceed to products or do not proceed directly to products without returning to the variational transition state (*12, 13, 54-57*). Recently, Hase and coworkers (*58*) have carried out trajectory calculations for reaction R2 starting from quantized energy distributions in the interaction region [this is called a quantized Keck calculation (*13*) in our earlier work]. They calculated a recrossing transmission coefficient of about 0.13 ± 0.07 at the conventional transition state for $T = 200$-2000 K (no systematic temperature dependence was observed). It is not known whether this effect would be smaller from the present potential function or if the dividing surface had been variationally optimized rather than placed at the conventional transition state. Ryaboy (*59*) has also suggested that recrossing effects may be important in S_N2 reactions. In the present work we account for recrossing of the conventional transition state to the extent that the canonical variational transition state theory rate is lower than the conventional one, but we do not include possible recrossing of the variational transition state. Inclusion of such effects may lower the predicted rate constants, and it may change the KIEs as well, but the estimation is beyond the scope of the present study. We note, however, that although classical recrossing effects are sometimes large, such effects are also sometimes (*12*, but not always, *60*) negligible in the real quantum mechanical world even when they are very significant in a classical mechanical world. The successes of quantized variational transition state theory with multidimensional tunneling corrections in the cases where it can be tested against accurate quantum dynamics (*1-8*) gives us some hope that it provides useful approximations for more complicated systems as well.

The final point to be discussed is quantum mechanical tunneling effects on the transmission coefficient. Our calculations recognize that at low energy, where tunneling is most important, all reactive flux is funneled through the ground state of the transition state. Thus we base our transmission coefficient on that state. Furthermore, in order to make the calculations practical for systems with many degrees of freedom, we perform them semiclassically. To calculate transmission coefficients accurately for the ground state of the transition state requires taking account of the multidimensional nature of the tunneling process. First of all, the optimum tunneling path is not the MEP. The MEP has the lowest barrier, but the optimum tunneling path involves a compromise between a low barrier and a short path. Since MEPs in mass-scaled cartesian coordinate systems are curved, tunneling paths tend to "cut the corner" (*18,19,50,61-69*) to shorten the

tunneling distance. The extent to which this occurs is a function of the curvature of the MEP when it is plotted in mass-scaled cartesians. In the small-curvature case (*18,50,61-65,70*), corner cutting, though quantitatively very important for the transmission coefficient, is relatively mild in terms of coordinate displacements. In this limit corner cutting tunneling has the nature of a negative bobsled effect due to a negative internal centrifugal potential arising from the curvature of the MEP. In this case accurate transmission coefficients can be calculated from a single path with an effective potential obtained by adding the local zero point energy to the potential energy along the MEP. (The sum is called the vibrationally adiabatic ground-state potential curve, where "vibrational adiabaticity" refers to the fact that the vibrational motion is in the local ground state.) Both the path and the effective potential depend on system masses. In the large-curvature case (*19,66-70*) corner cutting is severe, many paths must be considered, and the effective potentials are vibrationally adiabatic over part but not all of the paths. (In the nonadiabatic region the vibrational motion is not in the ground state, either physically or in the representation we use, but the semiclassical results are still referenced to the CVT results for the ground-state reaction.) The distribution of paths and the effective potentials again depend on system mass. Thus in neither limit does the mass enter so simply as in $\eta_{tun}^{\neq}$; consequently tunneling may be more important in the KIE than is conventionally assumed. In general one should consider tunneling into excited states in the exoergic direction in LCG3 calculations, but in the cases considered here, tunneling into excited states contributes at most a few percent.

We have developed a method, called the least-action ground-state (LAG) approximation (*13,20*), based on optimized tunneling paths, that is valid for small, medium, and large reaction path curvatures. We have also developed a centrifugal-dominant small-curvature semiclassical adiabatic ground-state (CD-SCSAG or, for short, small-curvature tunneling, SCT) approximation (*18,21,70*) and a large-curvature ground-state (called LCG3 or, for short, large-curvature tunneling, LCT) approximation (*13,21,26,70*), which are simpler and are expected to be accurate in the corresponding limits. Fortunately it is not usually necessary to perform full LAG optimizations; one obtains reasonable accuracy by simply carrying out both CD-SCSAG and LCG3 calculations and accepting whichever transmission coefficient is larger (since usually, though not always, both methods, at least where we have been able to test them against accurate quantum dynamics, underestimate the tunneling, and full LAG calculations have never been found to yield significantly more tunneling than the largest of the SCT and LCT limiting calculations). This is what we do here. In particular, although the systems discussed here were previously treated by the original (*18*) small-curvature approximation or by comparing this to LCG3 calculations considering only tunneling into the product ground state (*26*), all calculations have been updated for this chapter by performing CD-SCSAG calculations and LCG3 calculations including all energetically accessible final states in the exoergic direction for reaction R1 (and its isotopically substituted and reverse versions) and the ground final state for R2 and R3 (and their isotopically substituted versions), using methods discussed elsewhere (*70*), and accepting the larger of the two transmission coefficients at each temperature. The larger of the two results is simply labeled MT, which denotes multidimensional tunneling. In most cases the CD-SCSAG method yields the larger result, the exception being the unisotopically substituted version of reaction R2 with surface S. Individual transmission coefficients differ from those calculated by the original SCSAG method by as much as 31% for the cases considered here, but none of the kinetic isotope effects differs by more than 6% from those calculated with that method.

Factorization of the Kinetic Isotope Effect

For interpretative purposes we now require a new factorization of the per-site KIE, e.g., (3) is replaced by

$$\eta = \eta_{tun}\eta_{PF}\eta_{pot} \tag{8}$$

where

$$\eta_{tun} = \kappa_H^{MT}/\kappa_D^{MT} \tag{9}$$

$$\eta_{PF} = \frac{Q_H^{CVT}/\Phi_H^R}{Q_D^{CVT}/\Phi_D^R} \tag{10}$$

and

$$\eta_{pot} = e^{-\left(V_H^{CVT}-V_D^{CVT}\right)/RT} \tag{11}$$

Thus there is a critical distinction between the conventional TST and variational theory treatments. In conventional TST the transition state is at the same location (same structure) for both isotopes, and so the potential energy contributions cancel. Thus $\eta^{\neq} = \eta^{\neq}_{PF}$ and $\eta^{\neq}_{pot} = 1$. In variational TST this is not true. As a corollary, although the conventional TST rate constant may be computed from reactant and saddle point force fields that are both independent of mass, in variational TST the force fields used for the transition state partition function are different for the H and D versions of the reaction as a consequence of the change in structure.

For interpretative purposes we factor the partition function contribution η_{PF} to the variational TST value of the KIE into three further factors (*71,72*):

$$\eta_{PF} = \eta_{trans}\eta_{rot}\eta_{vib} \tag{12}$$

where the factors are due to translational, rotational, and vibrational partition functions. (Electronic partition functions are assumed to cancel, which is an excellent approximation.)

Applications

$H + CD_3H \rightarrow H_2 + CD_3$. The formalism reviewed above was applied (*27*) to the reaction of H with methane using a semiglobal analytic potential energy function, denoted J1, that was calibrated (*23*) previously. The form is an analytical function of 12 internal coordinates based on a functional form used earlier by Raff (*73*). The calibration (*23*) was based on the vibrational frequencies at the equilibrium geometries of CH_3 and CH_4 and at the saddle point, the heat of reaction at 0 K, the forward and reverse rate constants at 667K, and the equilibrium constant at 1340 K (*74-81*). The surface was also tested by calculating the primary KIEs which agree very well with experimental (*82-84*) values. The secondary deuterium KIE for CD_3H at 300K and its factorization are given in Table I. (In all cases, when we tabulate KIEs, they are the ratio of the rate constant for the isotopically unsubstituted reaction to that for the reaction of the isotopically substituted reagent under consideration.) In this table, TST/WT and TST/IPT denote conventional TST with one-dimensional transmission coefficients calculated respectively by the Wigner $\hbar^2$ tunneling correction (*85*) and by fitting the

potential energy along the MEP to an infinite parabola (*86,87*); the latter is sometimes called the Bell tunneling formula, but is here denoted infinite-parabola tunneling.

Table I shows several interesting results for this abstraction reaction. Conventional TST predicts a small KIE in the normal direction ($k_H/k_D > 1$), primarily because of rotational effects which are partly cancelled by an inverse vibrational effect. The conventional tunneling correction increases this KIE by only 3%. Variational transition state theory leads to a much larger KIE for the same potential energy function, and the vibrational contribution is now normal (> 1). Furthermore the tunneling contribution

Table I. KIEs and factors for $H + CD_3H \rightarrow H_2 + CD_3$ at 300 K

	η_{tun}	η_{trans}	η_{rot}	η_{vib}	η_{pot}	η
TST	···	1.01	1.27	0.83	···	1.07
TST/WT	1.01	"	"	"	···	1.08
TST/IPT	1.03	"	"	"	···	1.10
CVT	···	"	1.27	1.03	0.92	1.22
CVT/MT*	1.24	"	"	"	"	1.51

*denotes row used for further comparisons in Table V.

does not cancel out when its multidimensional aspects are included. Next we discuss the reasons why the variational effect on the overbarrier KIE is so large, raising the prediction from 1.07 to 1.22, and why the multidimensional tunneling contribution raises the predicted KIE still further, from 1.22 to 1.51.

The location of the variational transition state is determined mainly by competition between the potential energy $V_{MEP}(s)$ along the MEP and the zero point energy $\varepsilon^G_{int,2}(s)$ of one mode, ν_2 of the transition state. The frequency of the mode that correlates with this mode and $V_{MEP}(s)$ are given for four critical points along the MEP for the unsubstituted reaction in Table II. As this mode changes from a reactant stretch to a transition state stretch, it reaches a minimum of 1417 cm^{-1} shortly before the saddle point. By the time the saddle point is reached it is already increasing rapidly toward the product value of 4405 cm^{-1} (the harmonic stretching frequency of H_2 according to the J1 potential energy function). Thus, as the potential energy slowly begins to decrease from its stationary value at the saddle point, ν_2 is already raising rapidly. By the time the variational transition state has been reached, V has decreased only 0.1 kcal/mol, but $\varepsilon^G_{int,2}$ has increased 0.6 kcal/mol. At this point the free energy of activation is a maximum; beyond this the potential energy decreases faster than the zero point energy and generalized entropy of activation components increase. This behavior, which is illustrated in Figure 1, actually follows from simple bond-order arguments and was predicted qualitatively correctly in this way for a three-body model of this reaction years earlier (*88*).

Figure 2 shows the contributions of the various vibrational modes to the predicted KIEs at 300 K as calculated both at the saddle point and at the canonical variational transition state. (For degenerate modes the contribution shown is the total from both components.) Although ν_2 is the primary reason why the variational transition state is displaced from the saddle point, its own contribution to the KIE is the same for either location within 1%. The contributions of three other modes, however, differ by more than 7% (computed from the unrounded values), and this is the primary reason for the variational effect shown in Table I.

Figure 2 shows that there are indeed large contributions from the CH_3 bending and deformation modes (the modes at 1131-1379 cm^{-1}), as anticipated in the conventional discussions reviewed above, but the contributions of the other modes are by no means negligible, especially the H-H-C bend at 592 cm^{-1}. Furthermore two of the three CH_3 bending and deformation modes are among the modes whose contributions to the KIE are most sensitive to the variational optimization of the transition state.

The mass dependence of κ^{MT} appears to have two important sources. First, just including the mass-dependent zero point energies in the vibrationally adiabatic ground-state potential curve raises η_{tun} from the value of 1.03 in the Bell formula to 1.04. Second, accounting for corner cutting amplifies the transmission coefficient by a factor of 2.3 for H + H-CH_3 and by a factor of 2.0 for H + H-CD_3. This raises η_{tun} to 1.24.

Note that the imaginary-frequency normal mode at the saddle point has a frequency of 989i cm^{-1} for H-H-CH_3 and 981i cm^{-1} for H-H-CD_3. This small difference indicates that it is not necessary, as assumed in previous work (*40-42*) to have the C-D motions participate in the imaginary-frequency normal mode at the saddle point in order to have a significant secondary α-D kinetic isotope effect on the tunneling factor.

In order to test our model further, we can compare to experiment for two secondary kinetic isotope effects in this system, in particular, for $k_{CH_3+H_2}/k_{CD_3+H_2}$ and $k_{CH_3+D_2}/k_{CD_3+D_2}$. In both cases, the experimental value must be obtained indirectly by multiplying several other experimental ratios of rate constants. Based on the paper by Shapiro and Weston (*82*), we can use the scheme:

$$\frac{k_{CH_3+H_2}}{k_{CD_3+H_2}} = \frac{k_{CH_3+H_2}}{k_{CH_3+D_2}} \frac{k_{CH_3+D_2}}{k_{CH_3+A}} \frac{k_{CH_3+A}}{k_{CD_3+A-d_6}} \frac{k_{CD_3+A-d_6}}{k_{CD_3+H_2}} \qquad (13a)$$

$$= R_1R_2R_3R_4 \qquad (13b)$$

and

Table II. Reaction-path parameters for H + CH_4 → H_2 + CH_3

location	$V_{MEP}(s)$ (kcal/mol)	ν_2 (cm^{-1})	nature of mode ν_2
H + CH_4	0.0	3027[a]	H-C stretch
saddle point	13.0	1720	H-H-C stretch
variational transition state[b]	12.9	2195[a]	H-H-C stretch
H_2 + CH_3	2.8	4405[a]	H-H stretch

[a]This is the frequency of the mode that correlates with mode ν_2 of the transition state (see Figure I).
[b]300 K

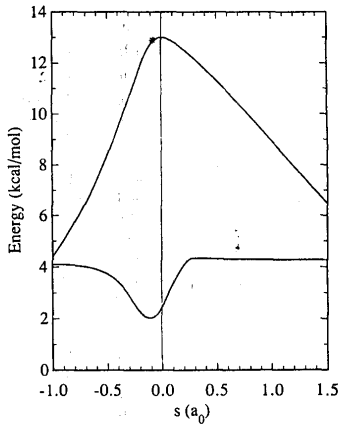

Figure 1. $V_{MEP}(s)$ and $\varepsilon^G_{int,2}(s)$ as functions (upper and lower curves, respectively) of s for reaction R1. The thin vertical line at s = 0 identifies the saddle point along the reaction coordinate, and the * identifies the V_{MEP} at the variational transition state at 300 K.

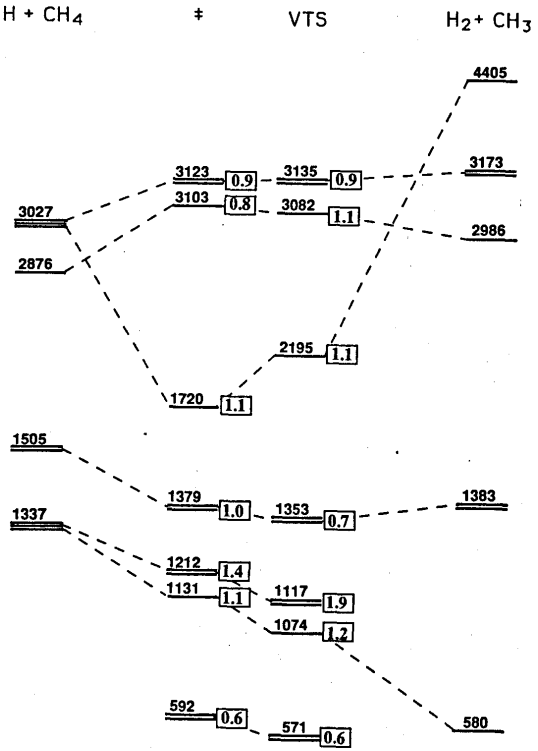

Figure 2. Frequencies (in cm^{-1}) and contributions to secondary KIEs (unitless numbers in boxes) for vibrational modes of (from left to right) H + CH_4, $CH_5^{\neq}$, CH_5^*, and H_2 + CH_3, where $\neq$ denotes the saddle point, and * denotes the variational transition state at 300 K.

$$\frac{k_{CH_3+D_2}}{k_{CD_3+D_2}} = \frac{k_{CH_3+D_2}}{k_{CH_3+A}} \frac{k_{CH_3+A}}{k_{CD_3+A-d_6}} \frac{k_{CD_3+A-d_6}}{k_{CD_3+H_2}} \frac{k_{CD_3+H_2}}{k_{CD_3+D_2}} \quad (14a)$$

$$= R_2R_3R_4R_5 \quad (14b)$$

where the ratios are defined R_1, R_2, ... in the order they appear in the line above. Note that A denotes acetone and A-d_6 denotes perdeuterated acetone. Shapiro and Weston measured R_1, R_2, R_4, and R_5, and using their values for these ratios and the value recommended in the review by Kerr and Parsonage (*89*) for R_3 yields a set of experimental results that we will call SW-KP. For comparison we also computed the experimental results using the values recommended by Kerr and Parsonage for R_1, R_2, and R_3 (*89,90*) combined with Shapiro and Weston's results for R_4 and R_5; these experimental values are labeled KP-SW. For a third set of values we used the more recent results of Arthur and Newitt (*91*) for k_{CH_3+A} in R_2 and for k_{CH_3+A} and $k_{CD_3+A\text{-}d_6}$ in R_3, again combined with the Kerr-Parsonage recommendations for R_1 and for $k_{CH_3+D_2}$ in R_2 and with Shapiro and Weston's values for R_4 and R_5; these experimental results are labelled AN-KP-SW. A fourth method, suggested by Weston (*92*), is to combine Shapiro and Weston's values for R_1, R_2, R_4, and R_5 with a value of R_3 calculated from the data analysis of Arthur and Newitt. This has the advantage that R_3 appears in both final ratios in the same way and thus does not affect the *relative* secondary KIEs for the H_2 and D_2 reactions. These results are called SW-AN. Comparison of these sets of experimental results provides an estimate of the error due to the uncertainty in R_1, R_2, and R_3. In addition to the variations in the table, which are due to R_1, R_2, and R_3, all values have an *additional* error contribution of 9-17% due to Shapiro and Weston's error estimates for R_4 and R_5. Table III also gives the theoretical results of Schatz *et al.* (*81*) and our calculations for three potential energy surfaces, J1, J2, and J3, all from Joseph *et al.* (*23*). For $k_{CH_3+H_2}/k_{CD_3+H_2}$, all calculations agree with experiment within the experimental uncertainty. For the D_2 reaction, the secondary deuterium kinetic isotope effects, $k_{CH_3+D_2}/k_{CD_3+D_2}$, are 19-31% smaller at 400 K, but the theoretical results are 8-10% smaller.

We do not know how reliable the experimental results are; it would be valuable to have experimental results obtained by an independent method. Such measurements would provide a valuable test of the theoretical predictions that the secondary kinetic isotope effect is only about 10% smaller for CH_3 + D_2 than for for CH_3 + H_2. There is, however, one clue (*92*) to the source of the disagreement between theory and experiment. As evidenced in Fig. 11 of the paper of Shapiro and Weston (*82*), the CD_3 + H_2/D_2 primary KIE, which is R_5, is low compared to the primary KIEs for CH_3 + H_2/D_2 and CF_3 + H_2/D_2. The same trend appears in the HD/DH primary KIEs. A low value for R_5 will change the secondary KIE for CH_3 + D_2/CD_3 + H_2 but does not affect the one for $k_{CH_3+H_2}/k_{CD_3+H_2}$. Thus it seems likely that there is some systematic error in the CD_3 experiments. As indicated in the derivation (*82*) of R_5, there are several corrections related to the H isotopic impurity in the acetone-d_6 used. Perhaps this is the source of error (*92*).

$^*Cl^-$ + CD_3Cl → $CD_3{}^*Cl$ + Cl^-. For the S_N2 exchange reaction of $^*Cl^-$ with CH_3Cl our results are based on an 18-dimensional semiglobal analytic potential energy function calibrated (*30*) to fit *ab initio* electronic structure calculations (*30,93,94*) of properties of the saddle point and ion-dipole complex, of energies, charges, and force fields on the MEP, and of energies at selected points off the MEP, to fit the correct long-range force law, and to fit one critical experimental datum, namely the rate constant for

Table III. KIEs for reverse of R1 and for analogous reaction with D_2

KIE	T(K)	theory				experiment			
		SWD	J1	J2	J3	SW-KP	KP-SW	AN-KP-SW	SW-AN
$k_{CH_3+H_2}/k_{CD_3+H_2}$	400	0.68[a]	0.67[a]	0.75	0.75				
		0.68[b]	0.82[c]	0.89	0.87	0.85	0.74	0.75	0.88
	500	0.77	0.77	0.84	0.83				
		0.77	0.87	0.94	0.92	0.86	0.86	0.82	0.85
	600	0.83	0.84	0.89	0.88				
		0.83	0.91	0.96	0.95	0.87	0.94	0.88	0.83
	700	0.87	0.87	0.92	0.92				
		0.87	0.94	0.99	0.97	0.88	1.00	0.92	0.81
$k_{CH_3+D_2}/k_{CD_3+D_2}$	400	0.68	0.67	0.75	0.74				
		0.68	0.74	0.81	0.80	0.59	0.60	0.60	0.61
	500	0.77	0.76	0.83	0.83				
		0.77	0.81	0.88	0.87	0.72	0.76	0.73	0.70
	600	0.84	0.82	0.88	0.88				
		0.84	0.87	0.93	0.92	0.82	0.89	0.83	0.78
	700	0.88	0.86	0.92	0.92				
		0.88	0.90	0.95	0.94	0.90	1.00	0.91	0.83

[a]Upper entry: conventional transition state theory with unit transmission coefficient. [b]Lower entry in SWD column: final result of Ref. 79 as obtained by conventional transition state theory with Wigner transmission coefficient. [c]Lower entry in J1, J2, and J3 columns: final results of this study as obtained by canonical variational theory with the CD-SCSAG transmission coefficient. All vibrational partition functions are calculated in the harmonic approximation for all calculations in the table.

the unsubstituted reaction at 300 K (*95*), which was used to adjust the *ab initio* barrier height. The final surface is called S because of this semiempirical adjustment.

A second set of calculations (*33*) was performed using the "direct dynamics" (*96*) approach. In this approach we do not parameterize an explicit potential energy function; rather we adjust the parameters in a semiempirical molecular orbital approximation to reproduce selected reaction features and the value of the potential energy function is defined implicitly by the energy yielded by the molecular orbital theory at any selected geometry. We selected the neglect-of-diatomic-differential-overlap (NDDO) level (*97-99*) of semiempirical molecular orbital theory, and we used the Austin model 1 (AM1) general parameter set (*100,101*) as our starting point. Then we readjusted two parameters (in particular, the one-electron, one-center atomic core matrix elements U_{pp} for Cl and C) specifically to energetic features assumed to be important for this S_N2 reaction. The resulting NDDO calculations with specific reaction parameters are called NDDO-SRP (*33*).

Table IV compares the KIEs for the CD_3Cl reaction (i.e., the ratio of the rate constant for the reaction in the section heading above to the rate constant with all protiums) and their factorizations for the two potential energy functions (PEFs). The results are remarkably similar, which tends to confirm the general correctness of both potential energy functions. In addition, the variational and conventional transition state theory results agree very well, and the tunneling contribution cancels out within one per cent (although the tunneling contribution is not negligible; $\kappa_H^{MT} = 1.31$ for both S and NDDO-SRP). Thus we can use any of the levels of dynamical theory in this case, and the same is true, within about 1%, for the KIEs in the microhydrated versions of this S_N2 reaction that are discussed below. Thus in the rest of the discussion of S_N2 reactions we will explicitly consider only the results at the most reliable (CVT/MT) level.

Table IV. KIEs and factors for $^*Cl^- + CD_3Cl \rightarrow CD_3{}^*Cl + Cl^-$ at 300 K

PEF	dynamics	η_{tun}	η_{trans}	η_{rot}	η_{vib}	η_{pot}	η
S	TST	...	1.04	1.22	0.76	...	0.96
	CVT	...	"	1.22	0.76	1.00	0.96
	CVT/MT*	1.00	"	"	"	"	0.96
NDDO-SRP	TST	...	"	1.23	0.75	...	0.96
	CVT	...	"	1.23	0.75	1.00	0.96
	CVT/MT	1.00	"	"	"	"	0.96

*denotes row used for further comparisons in Table V.

Table V shows a breakdown of the vibrational contribution to the KIE into contributions from three frequency ranges (for comparison, similar breakdowns for the other two KIEs discussed in this paper are also shown). As expected from the conventional interpretation of KIEs in S_N2 reactions (*38,39,43-45,102*), the contribution of the middle-frequency CH_3 bend and deformation modes is significant and > 1. However the low-frequency modes also contribute significantly, and the largest percentage deviation from unity comes from the high-frequency C-H stretches, which are almost universally ignored in discussions of secondary deuterium KIEs in the literature of the field. Perhaps some of the low KIEs observed experimentally which have been interpreted in terms of leaving group participation in tightening of the CH_3 bends and deformations are really caused to larger extent by stronger C-H bonds at the

sp^2 center. Certainly the correlated electronic-structure frequencies on which our saddle point C-H contributions are based are at least semiquantitatively reliable for the present case, and there can be no question that this effect exists and is very important.

At the finer level of detail exhibited in Table V, the NDDO-SRP results for $\eta_{vib,mid}$ and $\eta_{vib,high}$ differ from the presumably more accurate one calculated from surface S by 20-25% (from the NDDO-SRP calculations, we get 0.84 for $\eta_{vib,low}$, 1.01 for $\eta_{vib,mid}$, and 0.88 for $\eta_{vib,high}$), although as seen in Table IV, the differences eventually cancel. Nevertheless we are quite encouraged by the NDDO-SRP results since this method is very much easier to apply. In later work on $CF_3 + CH_4$ (Liu *et al.*, *36*), we are varying more parameters and paramaterizing to frequencies as well as energies, and we believe we can obtain even better potential energy functions by this method.

Table V. KIEs and factorization of η_{vib} at 300 K[a]

Reactants	$\eta_{vib,low}$	$\eta_{vib,mid}$	$\eta_{vib,high}$	η_{vib}	η
$H + CD_3H$	0.55	1.74	1.08	1.03	1.42
$Cl^- + CD_3Cl$	0.85	1.26	0.71	0.76	0.96
$Cl(D_2O)^- + CH_3Cl$	0.40	1.67	0.90	0.60	0.87

[a]In all cases the mode classification is based on the isotopically unsubstituted case. For the abstraction reaction the low/mid and mid/high borders are taken as 600 and 1700 cm^{-1}, respectively, and for the S_N2 reactions they are taken as 515 and 1900 cm^{-1}.

$^*Cl(D_2O)^- + CH_3Cl \rightarrow CH_3{}^*Cl + Cl(D_2O)^-$. When we add water of hydration, the PEF has three parts: solute, solvent, and solute-solvent interaction. We have used several different choices (*31,33,34*), and three of the combinations are summarized in Table VI along with the KIEs (i.e., the ratio of the rate constant for the reaction in the section heading above to the rate constant for all protiums) and their factorization. In the first calculations the solute was again treated by our semiempirical potential energy function S, the solute-solvent potentials were extended versions of the Kistenmacher-Popkie-Clementi (*103*) and Clementi-Cavallone-Scordamaglia (*104*) potentials, denoted eKPC and eCCS, respectively, and the intramolecular water potential was taken from Coker, Miller, and Watts (CMW, *105*). The second calculation was based on the NDDO-SRP method with no further changes in any parameters. The third is like the first except it is based on new chloride-water and intramolecular water potentials discussed in the next paragraph.

In carrying out calculations nos. 1 and 2 of Table VI we noted that the solvent KIEs are very sensitive to the low-frequency vibrations associated with the coupling of the solute to the solvent. Therefore, in work carried out in collaboration with Steckler (*106*), we calibrated a new potential energy function for $Cl(H_2O)^-$. The parameters of the new potential were determined to improve agreement with experiment for the dipole moment of water, with new extended-basis-set correlated electronic structure calculations for D_e, for the geometry and frequencies of the complex, for the individual and total vibrational contributions to the equilibrium isotope effect for $Cl(H_2O)^- + D_2O \rightleftarrows Cl(D_2O)^- + H_2O$, and for the energy at a geometry close to the saddle point geometry for reaction R_3, which is shown in Figure 3, and with the *ab initio* calculations of Dacre

Table VI. KIEs and factors for $^*Cl(D_2O)^- + CH_3Cl \rightarrow CH_3{}^*Cl + Cl(D_2O)^-$ at 300 K

		PEF								
No.	solute	$Cl\text{-}H_2O$	$CH_3\text{-}H_2O$	H_2O	η_{tun}	η_{trans}	η_{rot}	η_{vib}	η_{pot}	η
1.	S	eKPC	eCCS	CMW	1.00	1.03	1.41	0.72	1.00	1.04
2.	NDDO-SRP	NDDO-SRP	NDDO-SRP	NDDO-SRP	1.00	"	1.43	0.63	1.00	0.93
3.*	S	ZGTS	eCCS	mKH	1.00	"	1.41	0.60	1.00	0.87

*denotes row used for further comparisons in Table V.

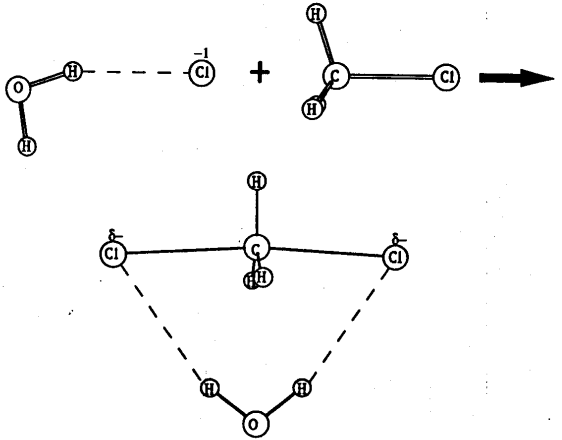

Figure 3. Structures of reactants and transition state for $Cl^-(H_2O) + CH_3Cl \rightarrow ClCH_3Cl^-(H_2O)^{\neq}$, based on the ZGTS chloride-water potential and the mKH intramolecular water potential.

(*107*) for the interaction energy of Cl^- with water at 369 widely distributed reaction sites. The chloride-water part of the interaction potential is totally new, and the intramolecular water part is a modified version (denoted mKH) of the accurate force field fit to spectroscopic data by Kauppi and Halonen (*108*), the modification being a change in the cubic O-H stretching force constants to get the red shift correct in the $Cl(H_2O)^-$ complex.

Table VI shows that calculations nos. 2 and 3 are in encouraging agreement with each other, and both predict an inverse KIE. The change from calculation no. 1 to no. 3 can be accomplished in 3 steps, and it is instructive to do so, as follows: First we change the CMW water potential to the original Kauppi-Halonen one, and this changes η from 1.04 to 0.97. Then we change the eKPC chloride-water potential to our new one based on the correlated $Cl(H_2O)^-$ calculations, and this decreases η further to 0.89. Finally, using the mKH water potential instead of the original Kauppi-Halonen one lowers η to 0.87.

Table V shows the more detailed factorization of η_{vib}. The biggest difference from the NDDO-SRP potential is in $\eta_{vib,low}$ (0.40 vs. 0.46), and the biggest difference from calculations no. 1 is in $\eta_{vib,high}$ (0.90 vs. 1.00). As a final comment, we note that the standard theory (*109,110*) of solvent kinetic isotope effects in the bulk is based on "water structure breaking" by ions, by which one means that the water librations are in a looser force field in the first hydration shell than in bulk (*111*). In our reaction, as seen in Figure 3, charge is delocalized at the transition state, so presumably, in bulk water, the water molecules would be in a tighter force field at the transition state than at reactants. Thus the bulk solvent KIE would be inverse. We also find an inverse result for a single water molecule, where water structure breaking is obviously impossible. Thus water structure breaking certainly cannot be the sole reason for the inverse KIEs observed in bulk solvent kinetic isotope effects.

Concluding remarks

Since the time when Shiner (*102*) summarized the interpretation of secondary kinetic isotope effects in an earlier ACS Symposium, there has been considerable progress. Both our force fields and our dynamics techniques have improved, and the reliability of our interpretations should correspondingly be much higher.

The techniques presented here are applicable to systems with many degrees of freedom. For example, the reaction $^*Cl(H_2O)_2^- + CH_3Cl$, which we have treated (*31,33*), has 12 atoms, and these techniques have been applied elsewhere to kinetic isotope effects in an embedded cluster with 29 non-fixed atoms (*112*), an intramolecular process with 7 atoms (*113*), a bimolecular neutral reaction with 9 atoms (*36*), and an intramolecular process with 13 atoms (*114*).

Acknowledgments

The authors are grateful to Bruce Garrett, Al Wagner, and Ralph Weston for helpful comments. This work was supported in part by the U. S. Department of Energy, Office of Basic Energy Sciences.

References

1. Truhlar, D. G.; Hase, W. L.; Hynes, J. T. *J. Phys. Chem.* **1983**, *87*, 2664, 5523E.
2. Garrett, B. C.; Truhlar, D. G. *J. Chem. Phys.* **1984**, *81*, 309.
3. Garrett, B. C.; Truhlar, D. G.; Schatz, G. C. *J. Amer. Chem. Soc.* **1986**, *108*, 2876.

4. Zhang, J. Z. H.; Zhang, Y.; Kouri, D. J.; Garrett, B. C.; Haug, K.; Schwenke, D. W.; Truhlar, D. G. *Faraday Discussions Chem. Soc.* **1987**, *84*, 371.
5. Lynch, G. C.; Truhlar, D. G.; Garrett, B. C. *J. Chem. Phys.* **1989**, *90*, 3110.
6. Lynch, G. C.; Halvick, P.; Truhlar, D. G.; Garrett, B. C.; Schwenke, D. W.; Kouri, D. J. Z. *Naturforsch.*, **1989**, *44a*, 427.
7. Schatz, G. C.; Amaee, B.; Connor, J. N. L. *J. Chem. Phys.*, **1990**, *93*, 5544.
8. Garrett, B. C.; Truhlar, D. G. *J. Phys. Chem.*, in press.
9. Bowman, J. M. *J. Phys. Chem.* **1991**, *95*, 4960.
10. Garrett, B. C.; Truhlar, D. G.; Bowman, J. M.; Wagner, A. F.; Robie, D.; Arepalli, S.; Presser, N.; Gordon, R. J. *J. Amer. Chem. Soc.* **1986**, *108*, 3515.
11. Garrett, B. C.; Truhlar, D. G. *J. Chem. Phys.* **1979**, *70*, 1593.
12. Truhlar, D. G.; Garrett, B. C. *Accounts Chem. Res.* **1980**, *13*, 440.
13. Truhlar, D. G.; Isaacson, A. D.; Garrett, B. C. In *Theory of Chemical Reaction Dynamics*; Baer, M., Ed.; CRC Press: Boca Raton, 1985; Vol. 4, p. 65.
14. Truhlar, D. G.; Garrett, B. C. *Annu. Rev. Phys. Chem.* **1984**, *35*, 159.
15. Truhlar, D. G.; Garrett, B. C. *J. Chim. Phys.* **1987**, *84*, 365.
16. Tucker, S. C.; Truhlar, D. G. In *New Theoretical Concepts for Understanding Organic Reactions*; Bertrán, J., Csizmadia, I. G., Eds.; Kluwer: Dordrecht, 1989, p. 291.
17. Garrett, B. C.; Truhlar, D. G.; Grev, R. S.; Magnuson, A. W. *J. Phys. Chem.* **1980**, *84*, 1730.
18. Skodje, R. T.; Truhlar, D. G.; Garrett, B. C. *J. Phys. Chem.* **1981**, *85*, 3019.
19. Garrett, B. C.; Truhlar, D. G.; Wagner, A. F.; Dunning, T. H. *J. Chem. Phys.* **1983**, *78*, 4400.
20. Garrett, B. C.; Truhlar, D. G. *J. Chem. Phys.* **1983**, *79*, 4931.
21. Truhlar, D. G.; Brown, F. B.; Steckler, R.; Isaacson, A. D. In *The Theory of Chemical Reaction Dynamics*; Clary, D. C., Ed.; Reidel: Dordrecht, 1986, p. 285.
22. Steckler, R.; Dykema, K. J.; Brown, F. B.; Hancock, G. C.; Truhlar, D. G.; Valencich, T. *J. Chem. Phys.* **1987**, *87*, 7024.
23. Joseph, T.; Steckler, R.; Truhlar, D. G. *J. Chem. Phys.* **1987**, *87*, 7036.
24. Garrett, B. C.; Redmon, M. J.; Steckler, R.; Truhlar, D. G.; Baldridge, K. K.; Bartol, D.; Schmidt, M. W.; Gordon, M. S. *J. Phys. Chem.* **1988**, *92*, 1476.
25. Baldridge, K. K.; Gordon, M. S.; Steckler, R.; Truhlar, D. G. *J. Phys. Chem.* **1989**, *93*, 5107.
26. Garrett, B. C.; Joseph, T.; Truong, T. N.; Truhlar, D. G. *Chem. Phys.* **1989**, *136*, 271; **1990**, *140*, 207E.
27. Lu, D.-h.; Maurice, D.; Truhlar, D. G. *J. Amer. Chem. Soc.* **1990**, *112*, 6206.
28. Natanson, G. A.; Garrett, B. C.; Truong, T. N.; Joseph, T.; Truhlar, D. G. *J. Chem. Phys.* **1991**, *94*, 7875.
29. Gonzalez-Lafont, A.; Truong, T. N.; Truhlar, D. G. *J. Chem. Phys.*, in press.
30. Tucker, S. C.; Truhlar, D. G. *J. Amer. Chem. Soc.* **1990**, *112*, 3338.
31. Tucker, S. C.; Truhlar, D. G. *J. Amer. Chem. Soc.* **1990**, *112*, 3347.
32. Zhao, X. G.; Tucker, S. C.; Truhlar, D. G. *J. Amer. Chem. Soc.* **1991**, *113*, 826.
33. Gonzalez-Lafont, A.; Truong, T. N.; Truhlar, D. G. *J. Phys. Chem.* **1991**, *95*, 4618.
34. Zhao, X. G.; Lu, D.-h.; Liu, Y.-P.; Lynch, G. C.; Truhlar, D. G., to be published.
35. Truong, T. N.; Truhlar, D. G. *J. Chem. Phys.* **1990**, *93*, 1761.
36. Liu, Y.-P.; Lu, D.-h.; Gonzalez-Lafont, A.; Truhlar, D. G.; Garrett, B. C., unpublished.
37. Johnston, H. S. *Gas Phase Reaction Rate Theory*, Ronald Press: New York, 1966.

38. Melander, L.; Saunders, W. H. Jr. *Reaction Rates of Isotopic Moleucles* (John Wiley & Sons: New York, 1980).
39. Saunders, W. H. Jr. In *Investigation of Rates and Mechanisms of Reactions (Techniques of Chemistry*, 4th ed., Vol. VI), Bernasconi, C. F., Ed.; John Wiley & Sons: New York, 1986, Part I, p. 565.
40. Ostović, D.; Roberts, R. M. G.; Kreevoy, M. M. *J. Amer. Chem. Soc.* **1983**, *105*, 7629.
41. Huskey, W. P.; Schowen, R. L. *J. Amer. Chem. Soc.* **1983**, *105*, 5704.
42. Saunders, W. H., Jr. *J. Amer. Chem. Soc.* **1985**, *107*, 164.
43. Streitwieser, A.; Jagow, R. H.; Fahey, R. C.; Suzuki, S. *J. Amer. Chem. Soc.* **1958**, *80*, 2326.
44. Scheppele, S. E. *Chem. Rev.* **1972**, *72*, 511.
45. Bentley, T. W., Schleyer, P. v. R. *Adv. Phys. Org. Chem.* **1977**, *14*, 1.
46. Wolfsberg, M.; Stern, M. J. *Pure Appl. Chem.* **1964**, *8*, 325.
47. Lim, C; Truhlar, D. G. *J. Phys. Chem.* **1986**, **90**, 2616.
48. Truhlar, D. G. *J. Phys. Chem.* **1979**, *83*, 199.
49. Shavitt, I. University of Wisconsin Theoretical Chemistry Laboratory Report WIS-AEC-23, Madison, 1959.
50. Marcus, R. A. *J. Chem. Phys.* **1966**, *45*, 4493.
51. Marcus, R. A. *J. Chem. Phys.* **1968**, *49*, 2610.
52. Truhlar, D. G.; Kuppermann, A. *J. Amer. Chem. Soc.* **1971**, *93*, 1840.
53. Fukui, K. In *The World of Quantum Chemistry*, Daude, R., Pullman, B., Eds.; Reidel: Dordrecht, The Netherlands, 1974, p. 113.
54. Keck, J. C. *Adv. Chem. Phys.* **1967**, *13*, 85.
55. Garrett, B. C.; Truhlar, D. G. *J. Phys. Chem.* **1979**, *83*, 1052; **1983**, *87*, 4553E.
56. Garrett, B. C.; Truhlar, D. G. *J. Phys. Chem.* **1980**, *84*, 805.
57. Garrett, B. C.; Truhlar, D. G.; Grev, R. S. *J. Phys. Chem.* **1981**, *85*, 1569.
58. Cho, Y. J.; Vande Linde, S. R.; Hase, W. L., to be published.
59. Ryaboy, V. M. *Chem. Phys. Lett.* **1989**, *159*, 371.
60. Truhlar, D. G.; Garrett, B. C. *Faraday Discuss. Chem. Soc.* 1987, *84*, 464.
61. Marcus, R. A. *J. Chem. Phys.* **1964**, *41*, 610.
62. Coltrin, M. E.; Marcus, R. A. *J. Chem. Phys.* **1977**, *67*, 2609.
63. Garrett, B. C.; Truhlar, D. G. *J. Phys. Chem.* **1979**, *83*, 200.
64. Garrett, B. C.; Truhlar, D. G. *Proc. Natl. Acad. Sci. USA* **1979**, *76*, 4755.
65. Skodje, R. T.; Truhlar, D. G.; Garrett, B. C. *J. Chem. Phys.* **1982**, *77*, 5955.
66. Babamov, V. K.; Marcus, R. A. *J. Chem. Phys.* **1978**, *74*, 1790.
67. Bondi, D. K.; Connor, J. N. L.; Garrett, B. C.; Truhlar, D. G. *J. Chem. Phys.* **1983**, *78*, 5981.
68. Garrett, B. C.; Abusalbi, N.; Kouri, D. J.; Truhlar, D. G. *J. Chem. Phys.* **1985**, *83*, 2252.
69. Kreevoy, M. M.; Ostović, D.; Truhlar, D. G.; Garrett, B. C. *J. Phys. Chem.* **1986**, *90*, 3766.
70. Lu. D.-h.; Truong, T. N.; Melissas, V. S.; Lynch, G. C.; Liu, Y.-P.; Garrett, B. C.; Steckler, R.; Isaacson, A. D.; Rai, S. N.; Hancock, G. C.; Lauderdale, J. G.; Joseph, T.; Truhlar, D. G. *Computer Phys. Commun.* to be published.
71. Garrett, B. C.; Truhlar, D. G.; Magnuson, A. W. *J. Chem. Phys.* **1982**, *76*, 2321.
72. Tucker, S. C.; Truhlar, D. G.; Garrett, B. C.; Isaacson, A. D. *J. Chem. Phys.* **1985**, *82*, 4102.
73. Raff, L. M. *J. Chem. Phys.* **1974**, *60*, 2220.
74. Kurylo, M. J.; Hollinden, G. A.; Timmons, R. B. *J. Chem. Phys.* **1970**, *52*, 1773.

75. *JANAF Thermochemical Tables*, 2nd ed.; Stull, D. R., Prophet, H., Eds.; U.S. Government Printing Office: Washington, 1971.
76. Shaw, R. *J. Phys. Chem. Ref. Data* **1978**, *7*, 1179.
77. Sepehrad, A.; Marshall, R. M.; Purnell, H. *J. Chem. Soc. Faraday Trans. 1* 1979, *75*, 835.
78. Walch, S. P. *J. Chem. Phys.* **1980**, *72*, 4932.
79. Schatz, G. C.; Walch, S. P.; Wagner, A. F. *J. Chem. Phys.* **1980**, *73*, 4536.
80. Sana, M.; Leroy, G.; Villareves, J. L. *Theoret. Chim. Acta* **1984**, *65*, 109.
81. Schatz, G. C.; Wagner, A. F.; Dunning, T. H. *J. Chem. Phys.* **1984**, **88**, 221.
82. Shapiro, J. S.; Weston, R. E., Jr. *J. Phys. Chem.* **1972**, *76*, 1669.
83. Rodriguez, A. E.; Pacey, P. D. *J. Phys. Chem.* **1986**, *90*, 6298.
84. Kobrinsky, P. C.; Pacey, P. D. *Can. J. Chem.* **1974**, *52*, 3665.
85. Wigner, E. P. *Z. Phys. Chem.* **1932**, *B19*, 203.
86. Bell, R. P. *The Tunnel Effect in Chemistry*, Chapman and Hall: London, 1980, pp. 60-63.
87. Skodje, R. T.; Truhlar, D. G. *J. Phys. Chem.* **1981**, *85*, 624.
88. Garrett, B. C.; Truhlar, D. G. *J. Amer. Chem. Soc.* **1979**, *101*, 4534.
89. Kerr, J. A.; Parsonage, M. J. "Evaluated Kinetic Data on Gas-Phase Hydrogen Transfer Reactions of Methyl Radicals," Butterworths, London, 1976.
90. The value recommended by Kerr and Parsonage for $k_{CH_3 + H_2}$ is also recommended in Tsang, W.; Hampson, R. F. *J. Phys. Chem. Ref. Data* **1986**, *15*, 1087.
91. Arthur, N. L.; Newitt, P. J. *Can J. Chem.* **1985**, *63*, 3486.
92. Weston, R., personal communication.
93. Chandrasekhar, J.; Smith, S. F.; Jorgensen, W. L. *J. Amer. Chem. Soc.* **1985**, *107*, 154.
94. Tucker, S. C.; Truhlar, D. G. *J. Phys. Chem.* **1989**, *93*, 8138.
95. Barlow, S. E.; Van Doren, J. M.; Bierbaum, V. M. *J. Amer. Chem. Soc.* **1988**, *106*, 7240.
96. Truhlar, D. G.; Gordon, M. S. *Science* **1990**, *249*, 491.
97. Pople J. A.; Santry, D.; Segal, G. *J. Chem. Phys.* **1965**, *43*, S129.
98. Pople, J. A.; Beveridge, D. J. *Approximate Molecular Orbital Theory* (McGraw-Hill, New York, 1970).
99. Dewar, M. J. S.; Thiel, W. *J. Amer. Chem. Soc.* **1977**, *99*, 4899, 4107.
100. Dewar, M. J. S.; Zoebisch, E. G.; Healy, E. F.; Stewart, J. J. P. *J. Amer. Chem. Soc.* **1985**, *107*, 3902.
101. Dewar, M. J. S.; Zoebisch, E. G. *J. Mol. Struc. (Theochem.)* **1988**, *180*, 1.
102. Shiner, V. J., Jr. *ACS Symp. Ser.* **1975**, *11*, 163.
103. Kistenmacher, H.; Popkie, H.; Clementi, E. *J. Chem. Phys.* **1973**, *59*, 5842.
104. Clementi, E.; Cavallone, F.; Scordamaglia, R. *J. Amer. Chem. Soc.* **1977**, *99*, 5531.
105. Coker, D. F.; Miller, R. E.; Watts, R. O. *J. Chem. Phys.* **1985**, *82*, 3554.
106. Zhao, X. G.; Gonzalez-Lafont; Truhlar, D. G.; Steckler, R. *J. Chem. Phys.* **1991**, *94*, 5544.
107. Dacre, P. D. *Mol. Phys.* **1984**, *51*, 633.
108. Kauppi, E.; Halonen, L. *J. Phys. Chem.* **1990**, *94*, 5779.
109. Swain, C. G.; Bader, R. F. *Tetrahedron* **1960**, *10*, 182, 200.
110. Schowen, R. L. *Progr. Phys. Org. Chem.* **1972**, *9*, 275.
111. Collins, K. D.; Washabaugh, M. W. *Quart. Rev. Biophys.* **1985**, *18*, 323.
112. Truong, T. N.; Truhlar, D. G. *J. Chem. Phys.* **1988**, *88*, 6611.
113. Truong, T. N.; McCammon, J. A. *J. Amer. Chem. Soc.*, submitted.
114. Lynch, G. C.; Liu, Y.-P.; Lu, D.-h.; Truong, T. N.; Truhlar, D. G.; Garrett, B. C., unpublished.

RECEIVED October 3, 1991

ACS SYMPOSIUM SERIES 502

Isotope Effects in Gas-Phase Chemistry

Jack A. Kaye, EDITOR
National Aeronautics and Space Administration

Developed from a symposium sponsored
by the Division of Physical Chemistry
at the 201st National Meeting
of the American Chemical Society,
Atlanta, Georgia,
April 14–19, 1991

American Chemical Society, Washington, DC 1992